frontiers | Frontiers in Environmental Science

TYPE Original Research
PUBLISHED 12 December 2022
DOI 10.3389/fenvs.2022.1094404

OPEN ACCESS

EDITED BY
Zhiyuan Hu,
School of atmospheric sciences, Sun Yat-sen University, China

REVIEWED BY
Wei Han,
CMA Earth System Modeling and Prediction Center, China
Hongsheng Zhang,
Peking University, China

*CORRESPONDENCE
Jizhi Wang,
jzwang@cma.gov.cn

SPECIALTY SECTION
This article was submitted to Atmosphere and Climate, a section of the journal Frontiers in Environmental Science

RECEIVED 10 November 2022
ACCEPTED 24 November 2022
PUBLISHED 12 December 2022

CITATION
Liu L, Zhang X, Wang J, Yang Y, Jia W, Zhong J, Jiang X and Wang Y (2022), Changes in the height of the pollution boundary layer and their meteorological effects on the distribution of surface ozone concentrations.
Front. Environ. Sci. 10:1094404.
doi: 10.3389/fenvs.2022.1094404

Changes in the height of the pollution boundary layer and their meteorological effects on the distribution of surface ozone concentrations

Liangke Liu[1], Xiaoye Zhang[2], Jizhi Wang[2]*, Yuanqin Yang[2], Wenxing Jia[2], Junting Zhong[2], Xiaofe Jiang[3] and Yaqiang Wang[2]

[1]Department of Earth System Science, Tsinghua University, Beijing, China, [2]State Key Laboratory of Severe Weather and Key Laboratory of Atmospheric Chemistry of CMA, Chinese Academy of Meteorological Sciences, Beijing, China, [3]China Meteorological Administration Training Centre, Beijing, China

Focusing on the key air pollution regions in China by using hourly automatic weather data, ground-based and high-altitude meteorological sounding data, and near-surface O_3 monitoring data, here, we try to quantify the relationship between boundary layer meteorological condition and near-surface O_3 concentrations. The key meteorological element includes changes in solar zenith angle, cloud height, atmospheric condensation rate, and the associated change in the boundary layer height. We also try to better understand the mechanisms by which meteorological conditions affect near-surface O_3 concentrations, and it is found that the exponential increase in near-surface O_3 concentrations after sunrise (called the O_3 concentration entrainment, EZ) is meaningfully associated with exceeding the threshold of a water vapor condensation rate (f_c) that is often closely linked to a significant rise in the pollution boundary layer and that this proves to be diagnostically important for understanding the O_3 EZ. Diurnal variations in solar zenith angle and boundary layer height are key meteorological factors influencing the large increase in near-surface O_3 concentration entrainment.

KEYWORDS

entrainment ozone (EZ) effect, solar zenith angle changes, height of pollution mixing layer (H_PML), O_3 growth by power exponential law, the conversion of precursor of O_3

Highlights

- Threshold of *fc* for driving to the increments of O_3 in the entrainment ozone (EZ) effect
- Combined spike of LCL and pollution mixing layers after sunrise favors the EZ effect

- Power exponential conversion is a favorable meteorological condition for O_3 growth

1 Introduction

With the continuous reduction of fine particle concentrations, the air quality during heavy pollution in winter has improved significantly; however, the heavy pollution events of ozone (O_3) in summer have gradually increased, causing widespread concern among the scientific and technological community, government, and the public. It is well-known that O_3 is driven by photochemical reactions triggered by both direct and indirect solar radiation. Nevertheless, in most cases, there is some uncertainty in the calculation of the chemical mechanism compared to the actual O_3 observations. Based on the long-term observational data during 2015–2022 in three representative regions, namely, Beijing, Hangzhou, and Guangzhou, this study attempts to discuss the influence of meteorological conditions on O_3.

In recent years, surface O_3 pollution has tended to increase. Some progress has been made with regard to the effects of meteorological conditions on O_3 concentrations near the ground (Andreas and Jochen, 2004).

With rapid economic growth, increase in O_3 in the troposphere is an evident trend. Air quality observations in 74 cities of China, in recent years, linked the rise in regional O_3 concentrations to weather and climate factors. Under global warming, a high O_3 concentration in the lower atmosphere becomes a frequent event in the North China, Yangtze, and Pearl River deltas. In the summer of 2017, the air temperature was higher than normal across most of China. Under the persistent high temperature, O_3 pollution occurred in north, northeast, and northwest of China from 17–19 July. Particularly, it lasted longer over Beijing. Based on the data from the Beijing Environmental Protection Monitoring Center starting from May 2017, O_3 concentration began to increase from between 08:00 and 09:00 a.m. in the Beijing–Tianjin–Hebei region, and sometimes it continued to increase even till 12:00 p.m. lasting for about a month from 1 July, the primary pollutant over Beijing was O_3. At 14:00 on 25 June 2022, the O_3 concentration increased as high as 297 μg/m^3, which has been achieving record O_3 concentration in June for the past 10 years. The "excessively high O_3 readings" became a new focus of concern. Some studies claimed that sometimes $PM_{2.5}$ concentration decreases with increasing O_3 concentration at the same time. Although this assertion has given some food for thought, it still lacks in-depth studies and common understanding.

Therefore, the commonality interaction of the influence of atmospheric physical processes and photochemical reactions on ozone has made some progress. Recently, some studies on the contribution of meteorological conditions to O_3 concentration increase apart from chemical processes have been recognized. Using meteorological data from the period of June 2004 to July 2004 from the national park of the Tunisian coast, it is found that O_3 concentration variation in summer is closely related to weather elements such as air temperature, rainfall, and wind over the coastal region. Their experimental study suggested that the local environment and meteorological conditions significantly influence temporal and spatial variations in O_3 distribution (Mechergui et al., 2009). Alghamdi et al. investigated the effects of relevant meteorological variables on frequently high NO_2 and O_3 concentrations in the coastal cities of Saudi Arabia in 2012–2013. They discussed the influence of seasonal variations under meteorological conditions on the O_3 concentration and indicated that O_3 concentration values peak in the summer and drop in the winter (Andreas and Jochen 2004). In recent years, observations and calculations of heavy O_3 pollution in Hangzhou in YRD, Guangzhou in PRD, Chengdu in Sichuan, and Beijing in the North China Plain have shown the importance of meteorological conditions (Wang and Chai, 2002; Li CH. et al., 2015; Li J. et al., 2015; Hu YT. et al., 2016). Using data from two observing stations in the vicinity of Hong Kong (the stations represent an inland area and an offshore sea.), Wang et al. conducted an observational study on the concentrations of major air pollutants and secondary substances (O_3, NO, NO_2, and SO_2) on a synchronous basis.

On the basis of further studies of the composite PLAM (parameter linking air-quality to meteorological condition) index of meteorological conditions for O_3 pollution and *via* observational data analyses, we focused on the contribution of meteorological conditions to O_3 pollution in four pollution-sensitive areas: YRD, PRD, North China Plain, and Sichuan, which are frequently exposed to pollution caused by high O_3 concentrations, and investigated their commonalities and influence mechanisms, and an objective description of the regional and seasonal condition was given. Recently, this study explored how meteorological conditions contributed to O_3 pollution in all seasons on the basis of further studies of the PLAM index (Wang et al., 2019). Although some progress has been made in investigating the influences of meteorological conditions on air quality, in recent years, it remains in the qualitative analysis stage; model-based studies are found lacking in the objective description of the possible mechanism of meteorological contributions to O_3 pollution. It is particularly noteworthy that the mechanism of the influence of atmospheric microphysical processes on near-ground ozone needs to be further explored. In recent years, it has been necessary to analyze and study the influence of high-resolution atmospheric detection information on ozone concentration.

In densely populated areas with rapid economic growth, many hydrocarbons and nitrogen oxides are emitted into the atmosphere. As a strong oxidizing agent, O_3 plays an important role in several processes of atmospheric chemistry. There are many research findings about the mechanism of O_3 genesis from the perspective of atmospheric chemistry, making much progress in this aspect. For example, previous reports have linked O_3 to the

decomposition and oxidation of organic compounds, oxidation of SO_2, and transformation of NO_2. However, when NO_2 exists in the troposphere, it is easy to observe O_3 genesis under certain atmospheric conditions (Webb and Steven, 1986). Although the impacts of clouds and aerosols on the climate have been studied for decades, it remains a complex and unsolved problem. The aerosol effect on enhancing cloud albedo is often called the first aerosol indirect effect. For climate patterns with uncertainties, the impact of atmospheric clouds is important because it is difficult to exclude the influence of different surface fluxes on turbulence dynamics, including the impact of cloud characteristics on the O_3 concentrations; therefore, the influence of meteorological conditions on atmospheric surface O_3 concentrations needs to be carefully studied and diagnosed (Wang and McFarquhar, 2008).

From the perspective of the traditional photochemistry-based description of O_3 generation mechanism, it is well-known that O_3 is driven by photochemical reactions initiated by solar radiation (for sure including direct and indirect solar radiation). Most studies with a relatively higher citation rate suggest that the discussions on photo-dissociation dynamics based on solar radiation and diurnal variation of the O_3 peak value in the lower atmosphere are closely related to specific values of volatile organic compounds (VOCs) and nitrogen oxides (NO_X). The solar radiation causes photo-dissociation of NO_2, which is the initial reaction to form haze. A steady-state concentration of O_3 is expressed as follows (Eq. 1) (Madronich and Flocke, 1999; Textor et al., 2006):

$$[O_3] = \frac{j[NO_2]}{k[NO]}, \tag{1}$$

where j is the photolysis frequency of NO_2, k is the rate coefficient for the NO reaction, and the brackets denote the concentrations of O_3, NO_2, and NO. The aforementioned relationship of NO, NO_2, and O_3 is called a steady-state relationship. Its dynamic equation is also given by Eq. 2 (Tang et al., 2006), which shows the solar radiation causes photo-dissociation of NO_2, which is the initial reaction to form smog. Its dynamic equation is given also as follows (Tang et al., 2006):

$$[O_3] = \left\{\left[\left(\frac{k_1}{k_2}\right)^2 + 4\frac{k_1}{k_2}[NO_2]_0\right]^{\frac{1}{2}} - \frac{k_1}{k_2}\right\}. \tag{2}$$

Here, the basic photochemical cycle of NO_2, NO, and O_3 is the fundamental source for O_3 genesis; k_1 and k_2 are the constants of transformation efficiency in chemical reactions; $\frac{k_1}{k_2} = 0.01 \times 10^{-6}$ can also be expressed as $\alpha = \frac{k_1}{k_2} \approx 0.01 \times 10^{-6}$ to describe the aforementioned transformation efficiency coefficient.

Nevertheless, recent findings show that the observed concentration of O_3 transformed from NO_2 is much larger than that given in Eq. 2. This allows us to speculate that some other factors beyond photochemistry in the troposphere may contribute to the high O_3 concentration.

As mentioned previously, the chemical mechanism of O_3 is an approximation. Values j or k and α depend on molecular parameters (absorption cross sections and photo-dissociation quantum yields) that are specific to the photo-reaction of interest, and on the availability of solar radiation at any specific location in the atmosphere (Tang et al., 2006).

Therefore, influenced by solar radiation, the diurnal change of the atmosphere is one of the important characteristics of the influence of meteorological conditions on the spatio-temporal redistribution of aerosols. The effect of the diurnal change of the solar zenith angle on the O_3 generation efficiency of light radiation in a specific region is the influence of the regional solar zenith angle diurnal meteorological conditions.

It is worth noting that Wallace and Hobbs proposed for the first time in their second edition of < Atmospheric Science > that during the destruction of the temperature inversion layer before and after sunrise, a consistency concept that the atmospheric lifting condensation level (LCL) variation in line with the height of the boundary layer (the height of the pollution mixing layer) can be increased rapidly as the solar zenith angle changes to a particular stage. They pointed out why it is closely related to the entrained O_3 layer (EZ) and the height of this polluting mixed layer (Wallace and Hobbs, 2006; Wang et al., 2017). However, research and observational information in this area are very scarce.

The intensity of solar ultraviolet radiation, the atmospheric channel of sunlight, and especially the impact of near-surface atmospheric meteorological conditions are extremely important factors affecting the troposphere O_3. When the solar zenith angle changes, the reflection path length of solar radiation passing through clouds with different structures naturally changes, which affects the O_3 content in the atmosphere (Browning, 1973; Bohn et al., 2008). Changes in cloud structure and solar zenith angles have superimposed and feedback effects on O_3 concentration. It not only drives the height change of the mixed pollution layer before and after sunrise but could also likely accompany the "EZ" process to further update the spatio-temporal distribution and change of O_3 concentrations. However, there is also a lack of data and research on these aspects.

In this study, we aim to explore the relationship between cloud height, atmospheric condensation rate, and solar zenith angle change based on the analysis of high-resolution information and calculation and explore the height change of the mixed layer of atmospheric pollution and its influence on the distribution of the surface O_3 concentration.

2 Data methodology

2.1 Data

This study uses hourly resolution automatic weather station (AWS) data, ground and high-altitude observation data from the

National Information Center (CMA) of the China Meteorological Administration, and atmospheric composition observations (http://www.zhb.gov.cn/hjzl/) of the Ministry of Ecology and Environment. In order to further study the spatio-temporal distribution of large-scale, persistent aerosol pollution, the parameters linking air-quality to meteorological conditions are discussed to indicate the spatial and temporal objective distribution of aerosol pollution (Wang et al., 2017). The parameters and calculation methods in this article are as follows.

2.2 Height of the pollution mixing layer

Hu et al. pointed out that while planetary boundary layer (PBL) parameterization is critical for air quality studies, constrained air quality simulations by PBL parametric schemes are not well-quantified under heavy fog pollution boundary layer conditions (Hu M. et al., 2016).

Currently, the way the boundary layer describes the effects of air pollution can be easily copied and can be confusing. For example, the PBL usually refers to the large-scale Ekman dynamic boundary layer. The concept of the PBL is simply used to assess the characteristics of air pollution associated with the near-surface boundary layer that may not be rigorous enough. For the measurement of heavy haze pollution, one of the selected functions of the parameterization scheme is to determine whether the air mass at a specific location meets the wet static stable state of "high humidity" but "rain is difficult to form" (Wallace and Hobbs, 2006; Wang et al., 2017). According to the definition of the wet potential temperature θ_e in Eq. 3, when the property in a particular layer (expressed by P coordinate) of the atmosphere reaches saturation, the saturation mixing ratio is W (W=W_s). Since R_d/C_p (0.288) is a constant in Eq. 3, under this height of the particular layer (expressed by P), it is very conducive for the continuous mixing of pollution when the condensation function f_c reaches the critical value of condensation. It should be noted that this is the threshold that needs to be captured, under the condition that the raindrops are yet to be formed.

That is, one of the functions of the air pollution meteorological conditions index is to indicate whether the local air masses are "stationary" with little variability. θ_e is an important parameter to characterize air mass properties (Holmboe et al., 1952; Yang et al., 1982):

$$\theta_e = \mathrm{T}\left[\left(\frac{1000}{\mathrm{P}}\right)^{\frac{R_d}{C_p}}\right]\exp\left[\left(\frac{Lw_s}{C_pT}\right)\right], \tag{3}$$

where C_p, L, w_s, and R_d are the meteorological parameters of specific heat with constant pressure, latent heat of water vapor condensation, saturation mixing ratio, and gas constant of the dry air, respectively.

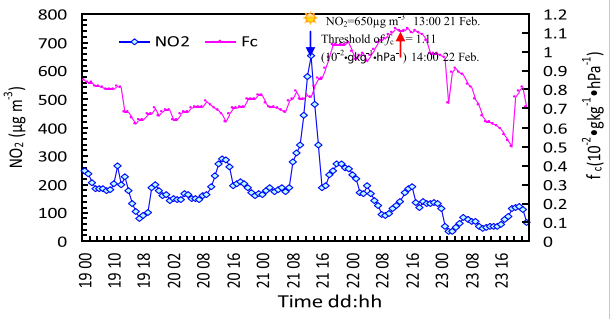

FIGURE 1
Evolution of the hourly condensation function f_c and NO_2 during the severe fog–haze process in Beijing in February 2001, "☀" represents the solar zenith angle for the local time (Zhang et al., 2005).

The processes and structures of the atmospheric micro-scale flow field, condensation, and mechanisms of clouds and precipitation are intrinsically linked. Much progress has been achieved in these aspects associated with air pollution contributions, as well as the emission disturbance changes under different meteorological conditions (Gao and Zhou, 2005; Wang et al., 2012). When the f_c reaches the critical value of condensation, but without raindrop formation, the atmosphere is very favorable for the continuation of pollution mixing, for the wetting of particles, and accelerating the formation of new particles for the generation of secondary pollution (Kulmala et al., 2004; Shen et al., 2016). At this time, it is necessary to pay attention to capturing "the threshold" related to humidity for a value that is high enough, but not too high. At this atmospheric layer height, the height of pollution mixing layer (H_PML), a precursor signal of air pollution, will appear (Wang et al., 2017).

$$H_{PML} \approx 6.11 \times 10^2 \left(\frac{0.622 + 0.622\frac{e_s}{p-e_s}}{0.622\frac{e_s}{p-e_s}}\right), \tag{4}$$

where e_s is the saturation water vapor pressure, that is, the capturing and calculation of the precursory signal of atmospheric pollution mixing layer height.

Wallace and Hobbes proposed first in their second edition of < Atmospheric Science > that during the period before and after sunrise, destruction of the inversion layer due to warming of the strata near the atmosphere results in an increase in atmospheric lifting condensation levels (LCLs), which causes the height of the LCL and the boundary layer and the height of the pollution mixing layer to converge to the same height. The height of the pollution mixing layer increases rapidly again as the solar zenith angle changes. This illustrates why the efficiency of the EZ is closely related to the height of the contaminated mixed layer (Wallace and Hobbs, 2006; Wang et al., 2017).

Trousdell et al. (2016) pointed out that the photochemical productivity of O_3 is closely related to the EZ rate of polluting mixed layers. EZ velocity is the parametric rate at which free tropospheric air is incorporated into the atmospheric boundary layer (ABL).

2.3 Atmospheric condensation and super-saturation

Zhang et al. (2005) discussed typical cases of heavy fog–haze processes and boundary layer characteristics in Beijing in 2001. The results showed that the threshold of condensation rate before and after the thick haze had a significant effect on the aerosol pollution of NO_2 and SO_2 concentration (see Figure 1).

The threshold of condensation rate was captured by the decrease of NOx as the O_3 precursor in the hourly resolution observations. As shown in Figure 1, from Beijing local time of 02: 00 on February 20 to 08:00 on February 22 in 2001, after a period of continuous elevation of the f_c for 48 h, severe haze appeared, and at 13:00 on 21 February 2002, when the solar zenith angle peaked, NO_2 was as high as 650, and f_c continued to increase to a threshold of up to 1.11. Subsequently, it quickly dropped to the lowest. This so called threshold value was high enough, but yet not too high (Zhang et al., 2005).

The expression of the condensation function (condensation rate) mentioned previously is given by Eq. 5 (Zhang et al., 2005):

$$\begin{cases} f_c = f_{cd} \Big/ \left[\left(1 + \dfrac{L}{C_p} \dfrac{\partial q_s}{\partial T} \right)_p \right] \\ f_{cd} = \left[\left(\dfrac{\partial q_s}{\partial P} \right)_T + \gamma_d \left(\dfrac{\partial q_s}{\partial T} \right)_p \right], \\ \gamma_d = \dfrac{R_d}{C_p} \dfrac{T}{P} \end{cases} \tag{5}$$

where γ_d is the dry insulation rate ($C^{\circ}m^{-1}$) and C_p, L, q_s, and f_{cd} are the meteorological parameters of the specific heat with constant pressure, latent heat of water vapor condensation, saturation specific humidity, and dry air condensation rate, respectively. The condensation function is a function of super-saturation (S). The super-saturation degree is a physical quantity that is expressed in percentage (Wang et al., 2017).

$$S = (e/e_s - 1) \times 100\%, \tag{6}$$

where e and e_s are the water vapor pressure and saturated water vapor pressure, respectively. That is, for the nature of air quality, under the condition of large-scale processes, with "uniformity" and "static" (iso-θe), and associated with the microphysical process of atmospheric condensation described by the appropriate f_c (threshold), the clouds, haze, and other weather conditions would occur differently. These parameters also coordinate with each other, creating a relationship of interdependence and mutual constraints (Wang et al., 2017). The studies have also suggested that the atmospheric condensation rate f_c, as a wet driver of micro-meteorological conditions, can accelerate and catalyze O_3 precursors to form secondary pollution. This power exponential conversion law describes changes in O_3 concentrations due to special micro-scale meteorological processes that is given as (Wang et al., 2019)

$$\delta O_3 = \alpha(\chi)^{-\beta}, \tag{7}$$

χ represents the O_3 precursor of NOx or VOCs, etc., β is the condensation function (f_c), and $\alpha \approx 10.0 \times 10^3$

3 Results and discussion

3.1 Characteristics of polluted weather and H_PML in Beijing, North China, from February 11 to 13, 2022

Figure 2A shows the observed distribution of an hour-by-hour O_3 in February 2022 and the hour-by-hour fluctuation in the pollution boundary layer height H_PML calculated by Eq. 4, and Figure 2B shows the observed distribution of hour-by-hour O_3 and the amplified detailed distribution of the H_PML fluctuations of the pollution boundary layer in Figure 2A from February 10 to 11. Figure 2C shows a weather map of the surface at 14:00 (BJT) on February 11. The figures indicate that

1) there was a significant daily change in the H_PML (red line), that is, the H_PML increased during the day and decreased at night. The peaks of the diurnal variation corresponded to the peaks of the O_3 concentration observed (green line).

As shown in Figure 2A, during the period February 10–15 and February 24–28, 2022, Beijing experienced two cases of smog (see the haze weather symbol at the bottom of Figure 2A), in which O_3 and $PM_{2.5}$ concentrations increased. There were two significantly polluted weather processes in February 2022 in Beijing, where the air quality dropped significantly. At 15:00 on 10 February 2022, an O_3 concentration of 96 μg/m^3 was observed, and at 14:00 on 11 February 2022, an O_3 concentration of 98 μg/m^3 was observed (see Figure 2B), and PM_{10} increased significantly. From February 8 to 13, the intermittent fog–haze weather in Beijing lasted for 120 h, and drifting snow was observed (large area of haze or snow weather occurred in and around Beijing) (see the surface weather map of Figure 2B). Beijing's fog–haze, gloomy low-visibility conditions affected the official schedule of some of the Winter Olympics events. At that time, the schedule of some events, including the women's U-shaped ski competition, was affected and got appropriately delayed.

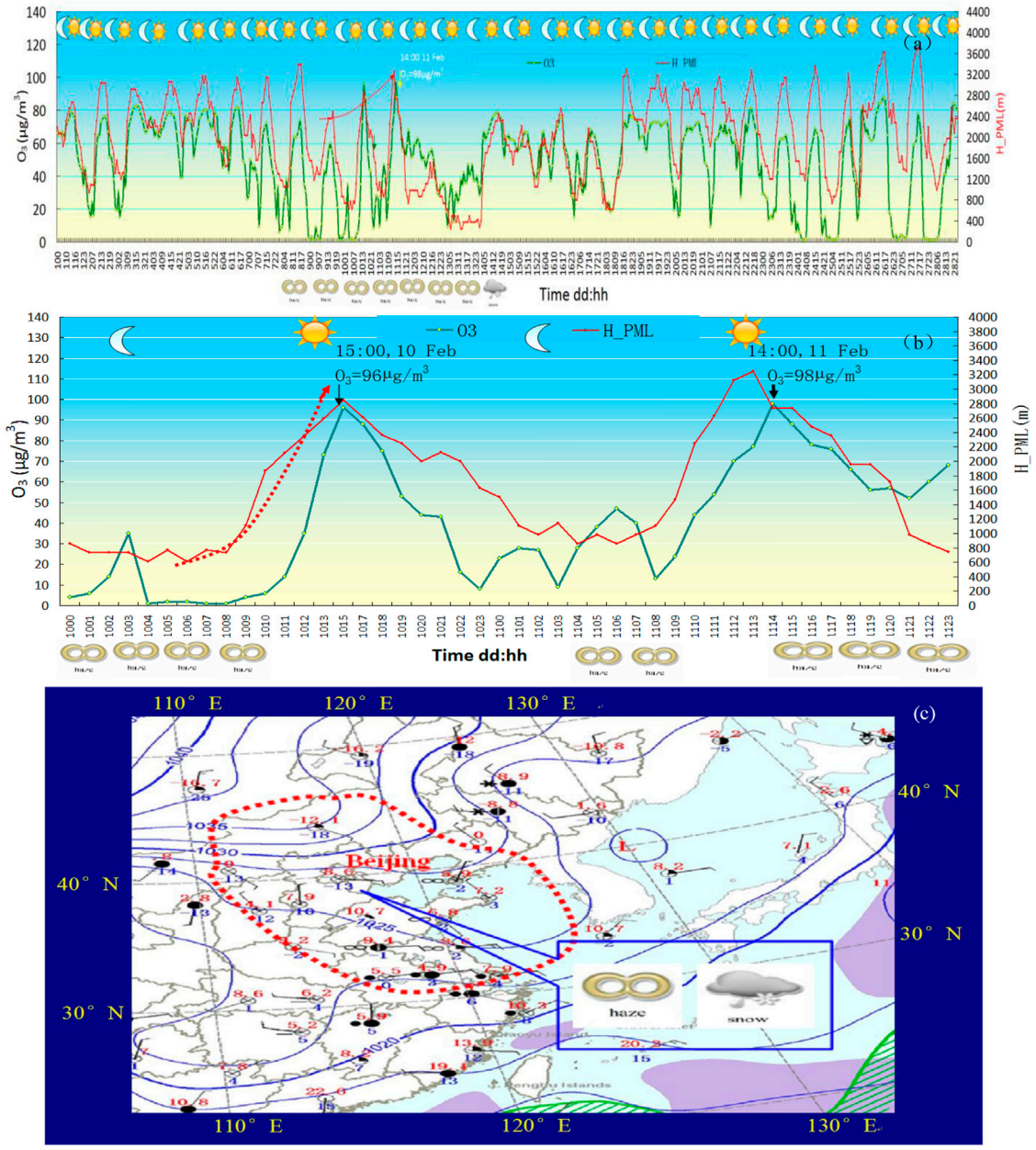

FIGURE 2
(A) Hour-by-hour O_3 and H_PML changes in February 2022 in Beijing, **(B)** hour-by-hour detailed distribution of O_3 and the height of H_PML fluctuations from December 10–11 in **(A)**, and **(C)** ground weather map at 14:00 (BJT) on February 11 in Beijing.

2) In February 2022, in addition to the significant daily changes in the height of the boundary layer (H_PML), a long period of continuous increase was noted. For example, at 05:00 on 10 February 2022, the peak with the H_PML continued to increase from 2,400 m to 2,900 m till 15:00 on February 10. Also, from 05:00–14:00 on February 11, it increased again to 3,252 m (see the dotted line arrow in Figure 2A).

3) It can be seen from Figure 2B that from the afternoon to evening the pollution developed rapidly and the air quality dropped significantly. In Figure 2B, the detailed distribution of day-to-day fluctuations in the H_PML of the pollution boundary layer from February 10 to 11 can be seen, and pollution developed rapidly from afternoon to evening, deteriorating the air quality significantly. On February 10, at 15:00, the O_3 concentration was observed to be 96 μg/m^{3,}

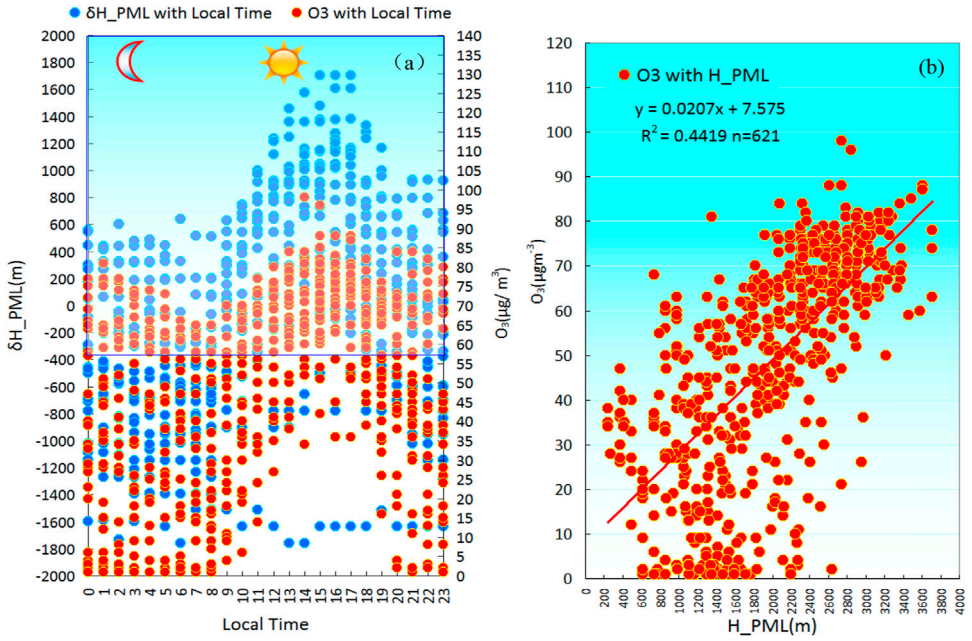

FIGURE 3
(A) Comprehensive analysis of O_3 and δH_PML at hourly resolution in Beijing in February 2022, where the δH-PML is the anomaly labeled as the average value of 2000 m. **(B)** Analysis of O_3 and H_PML with hourly resolution in Beijing in February 2022.

and from 0:00 to 10:00 on February 10, Beijing experienced continuous haze for 10 h. On February 11, from 4:00 to 23:00, the haze weather continued for nearly 20 h, the O_3 concentration observed at 14:00 was 98 μg/m^3 (see the weather symbol note at the bottom of Figure 2B and the haze weather symbol note at the bottom of Figure 2C, the ground weather map), the haze weather in Beijing and North China continued, and the sky conditions were obscure.

3.2 Analysis and calculation of the entrained ozone (EZ) rate and its associated increase in O_3 concentration by H_PML changes before and after sunrise

Studies indicated that during daytime over continents, when near-surface ozone (O_3) usually peaks, the convective thermal energy generated by surface heating rises and penetrates into the stable layer, which divides the interface attachment between the turbulent atmospheric boundary layer (ABL), or the so-called pollution mixing layer (PML), and the free troposphere (FT) (its height is so-called LFC) above it. The continuous action of these heats permeates the laminar-covered air and falls back to the pollution boundary layer, producing an irreversible mixing process that causes the layer to grow with the layers of LFC, i.e., the H_PWL is consistent with the height of the free troposphere (LFC). The whole process is called entrainment. When the two layers contain different amounts of any scalar quantities (e.g., ozone concentration, water vapor, and entropy), this mixture is often an important contributor to scalar PWL budgets (Albrecht et al., 2016).

Lenschow et al. argued that calculating the change in mixed layer height (zi) before and after sunrise can derive the entrainment velocity of increasing O_3, considering the relationship between the observed local ABL lifting rate and the average vertical velocity at the height of temperature inversion (Angevine, 1997; Lenschow et al., 1999). The aircraft-based study shows that ABL budgeting can help check regional emission rates and photochemical production rates. However, for the O_3 budget, a detailed comparison with the photochemical model reveals the obvious weaknesses in the current model, including an indication about whether the difficulty lies in the kinetics (transmission) or in the chemical aspects of numerical work. Evaluation of detection accuracy and associated huge cost are also among the constraints. However, as Wallace et al. mentioned previously, during the destruction of the temperature inversion layer around sunrise, the LCL variation in line with the height of the boundary layer and the height of the pollution mixing layer increases rapidly with a change in the solar zenith angle. It is convenient and reasonable to calculate the height changes of this polluting mixed layer. Eq. 4 (for calculating the H_PML) can be used to

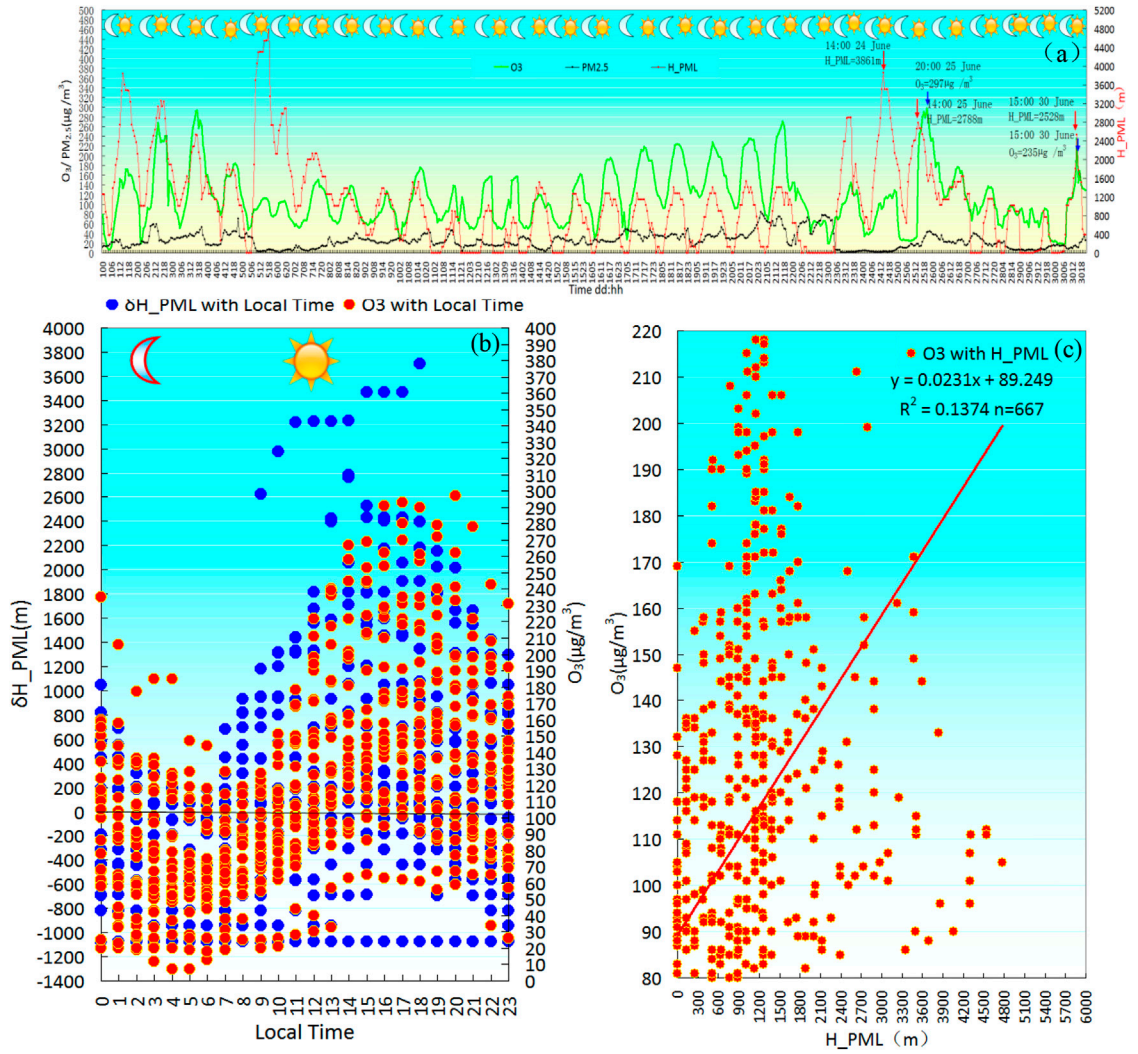

FIGURE 4
(A) Observed distribution of hour-by-hour O_3 in June 2022 in Beijing and daytime fluctuations in the pollution boundary layer height H-PML calculated by Eq. 4, as well as hourly changes of $PM_{2.5}$. **(B)** Comprehensive analysis of O_3 and δH_PML at the local time of hourly resolution in June 2022 in Beijing, The ordinate (left) is for δH-PML, where the δH-PML is the anomaly labeled as the average value of 1000 m. **(C)** Correlation between the hourly O_3 and H_PML in June 2022 in Beijing.

link with the entrainment velocity of O_3 growth. By using Eq.7, the increasing O_3 driven by the threshold f_c before and after sunrise can be calculated so that it can also be reasonable to calculate the EZ rate of polluting mixed layers, which is associated with the increased O_3 concentration.

3.2.1 Correlation characteristics between O_3 pollution and H_PML in Beijing in February 2022

Figure 3A is a comprehensive analysis of an hour-based resolution of daily-evolution of O_3 in the local time, as well as H_PML in February 2022 in Beijing, while Figure 3B shows the correlation between hourly O_3 and H_PML in February 2022 in Beijing. From Figure 3, we can see the following:

1) in the winter of February 2022, the comprehensive correlation analysis of daily local-time hourly O_3 and H_PML shows that as the change of the solar zenith angle has a remarkable and instant effect on the O_3 concentration, H_PML increased from 2,500 m (positive anomaly 500 m, for average 2000 m) at 7:00 a.m. to 3,200 m (i.e., positive anomaly 1,200 m) at 12:00 noon (indicated by a blue dot in Figure 3A), with increase in the solar zenith angle during sunrise. Accordingly, O_3 concentrations increased from 65 μg/m^3 at 7:00 to 80 μg/m^3 at 12:00 p.m. Peaks at nearly 100 μg/m^3 were reached at 14:00 p.m. Such an O_3 concentration value is not common in Beijing in February during winter. It was shown that the EZ effect contributed significantly to the increase in O_3

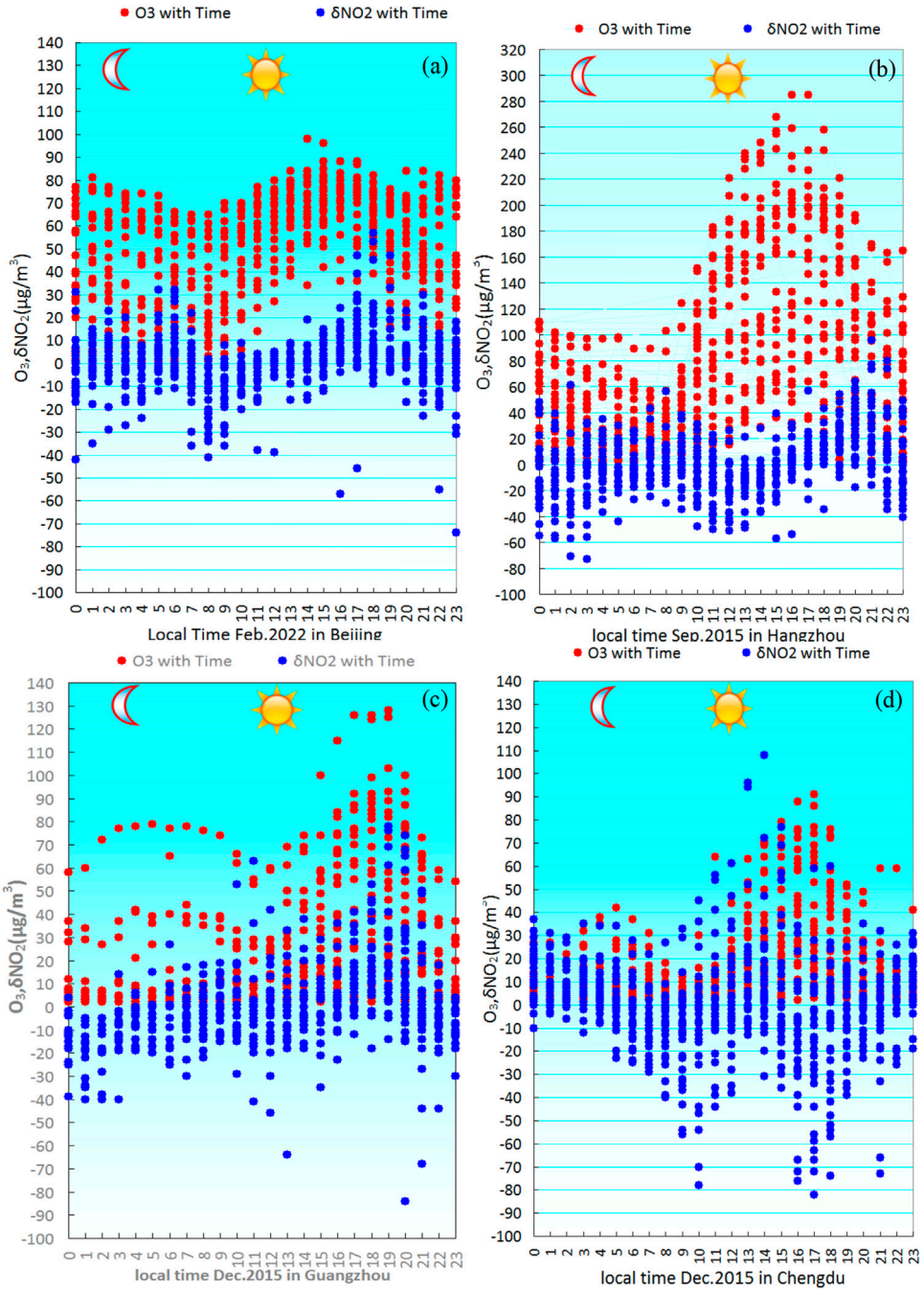

FIGURE 5
(A) Correlation comprehensive analysis of O_3 and δNO_2 in February 2022 hourly resolution local time in February 2022 in Beijing, **(B)** content is the same as **(A)**, the place and time of the shift is Hangzhou, September 2015, **(C)** content is the same, but the place and time are Guangzhou, December 2015, and **(D)** content is the same as **(A)**, the place and time are Chengdu in December 2015.

concentrations with the sharp rise of the pollution mixing layer after sunrise.

2) Correlation analysis of H_PML and O_3 concentrations in an hourly resolution in February (Figure 3B) shows that H_PML significantly positively correlated with O_3 concentrations. The correlation coefficient (R^2) was 0.44, which was significant at 0.001. A direct influence of the EZ effect on O_3 concentrations was further confirmed by the sharp rise of the concomitant pollution mixing layer after sunrise (Figure 3A).

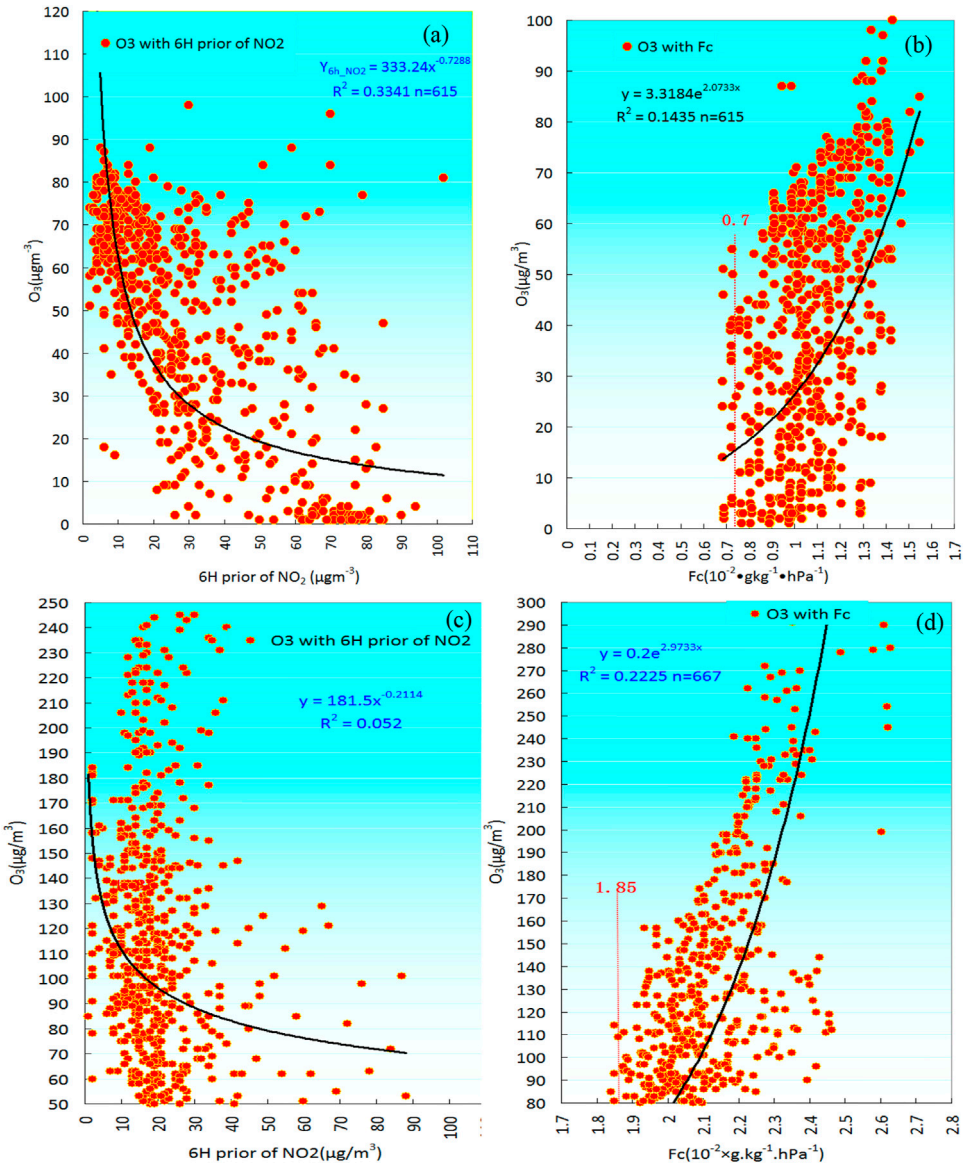

FIGURE 6
(A) Correlation analysis of the hourly resolution O_3 and NO_2 before 6H in Beijing in February 2022, **(B)** correlation analysis between the hourly resolution O_3 and condensation function (f_c) in February 2022, **(C)** content is the same as **(A)**, but the time is June 2022 in Beijing, and **(D)** content is the same as **(B)**, but the time is June 2022 in Beijing.

3.2.2 Correlation characteristics between O_3 pollution and H_PML in Beijing in June 2022

Figure 4A shows the hourly variations of O_3 in June 2022 and the daytime fluctuations in the H_PML calculated by Eq. 4, as well as the hourly change in $PM_{2.5}$. Figure 4B shows the comprehensive analysis between hourly O_3 and δH_PML in June 2022 with the left ordinate being δH-PML, where the δH-PML is the anomaly labeled as the average value of 1000 m. Figure 4C is a correlation analysis of O_3 and H_PML based on the hourly resolution in local time in June 2022. Figure 4 indicates that

1) the solar altitude angle changed considerably with local time daily in the summer of June 2022. O_3 concentrations increased during the day and decreased at night.
2) For the typical month of heavy O_3 pollution in summer, the relevant comprehensive analysis of the daily local-time hourly resolution of O_3 and H_PML in June 2022 showed that the daily change of the solar zenith angle had a significant effect on the O_3 concentration than those in winter. H_PML of 1,600 m at 7:00 a.m. (600 m for the positive anomaly, the average value is for 1,000 m) reached 4,200 m (namely,

3,200 m for the positive anomaly) at 12:00 noon (Figure 4A blue dot), which was 1,000 m higher than that in February, and it further rose to 4,800 m again after 3 h. During sunrise, with the change in the solar zenith angle, the height of the pollution mixing layer H_PML sharply increased, which was calculated according to Eq. 4.

3) Correspondingly, O_3 concentrations increased from 150 μg/m^3 at 7:00 a.m. to 220 μg/m^3 at 12:00 p.m. A peak at nearly 300 μg/m^3 was observed at 20:00 p.m. This O_3 concentration value is rare, in recent years, in Beijing in June. It was shown that in summer, with the sharp rise of the pollution mixing layer after sunrise, the EZ effect contributed significantly to the increase in O_3 concentrations.
4) Correlation analysis of H_PML and hourly O_3 concentrations in June (Figure 4C) shows that H_PML significantly positively correlated with O_3 concentrations. The correlation coefficient (R^2) was 0.14, and it was significant at level 0.01. It is further confirmed that (Figures 4A,B) there is a sharp rise in the height of the sewage mixed layer after sunrise in summer.
5) The superimposed effect of the EZ contribution on the O_3 concentrations, driven by the changes in the local solar zenith angle, is an important reason for the ultra-high O_3 concentration in the summer of 2022. In Figure 4A, the increase in O_3 concentration driven by the change in solar zenith angle is synchronized with the increase in O_3 concentration due to the sharp rise in H_PML, and the proliferation of O_3 concentration is superimposed during the second half of June. At 14:00 on June 24, at the peak moment of the solar zenith angle, the H_PML sharply rose to 3,861 m, and 24 h later, at 14:00 on June 25, the O_3 concentration increased as high as 297 μg/m^3, achieving the record high O_3 concentration in June in the past 10 years.

3.2.3 Seasonal and regional characteristics of the contribution of EZ effect and solar zenith angle to the increase in O_3 concentration

To explore the universal significance of the contribution of the EZ effect on the enhancement of O_3 concentrations by solar zenith angle change to the height change of the pollution mixed layer, this section discusses the contribution characteristics of the EZ effect of each season at selected stations at Beijing, Hangzhou, Guangzhou, and Chengdu, which are representatives of the four typical polluted areas, *i.e.*, North China, Yangtze River Delta, the Pearl River Delta, and Sichuan Basin. Figure 5A shows a comprehensive analysis of O_3 and δNO_2 in Beijing in February 2022 at local hourly resolution. The contents in Figures 5B–D are the same, showing haze in Guangzhou in the winter of 2015, Chengdu in December 2015, and the transition season (autumn) in Hangzhou in September 2015. Figure 5 shows

1) the mega-cities such as Beijing, Hangzhou, Guangzhou, and Chengdu are densely populated and are representative stations of typical areas of air pollution in China, including O_3 pollution (Zhang et al., 2012). Figure 5 shows that the effects of the solar zenith angle diurnal changes to the height change of the pollution mixing layer on O_3 concentration hyperplasia are common in these four typical areas. The red dot indicates the O_3 concentration, and the high value appeared 3–5 h after the peak of the solar zenith angle.
2) O_3 concentration as high as 100 μg/m^3 in Beijing, North China, was observed in early spring and February, and in the typical winter of December 2015, O_3 pollution was heavier in Chengdu Basin area, reaching 140 μg/m^3 and in the Pearl River Delta reaching 90 μg/m^3.

However, in the autumn, the concentration of O_3 in the Hangzhou region of the Yangtze River Delta reached 300 μg/m^3.

3) An important common feature during the temperature inversion at night is that as the NO_2 concentration decreases, the O_3 concentration gradually increases, and during the peak period of the solar zenith angle (at 12:00 local time), the temperature inversion is destroyed, the O_3 jump is extremely rapid, and the peak of the O_3 appears at 15:00–17:00 p.m. This explains the link between the high degree of the pollution mixing layer and the solar zenith angle change.

The contribution of EZ effect to the increase of O_3 concentration due to the change of H_PML in the above-mentioned major impact regions of China (North China Plain, Yangtze River Delta, Pearl River Delta and Sichuan Basin), including the increase magnitude and lag time, is consistent with the variation of solar zenith angle. Thus, the meteorological impact has universal characteristics.

3.3 Correlation analysis of the power-exponential increase in O_3 concentration driven by the condensation function threshold

3.3.1 Contribution of NO_2 as an O_3 precursor on the power-exponential growth of O_3 concentration and the threshold of condensation function f_c

As mentioned previously, previous studies showed that solar radiation causes photo-dissociation of NO_2. However, thorough understanding on how NO_2 is influenced by meteorological conditions to generate O_3, the power exponent law of NO_2 conversion to O_3, and the driving mechanism of the f_c threshold is very important.

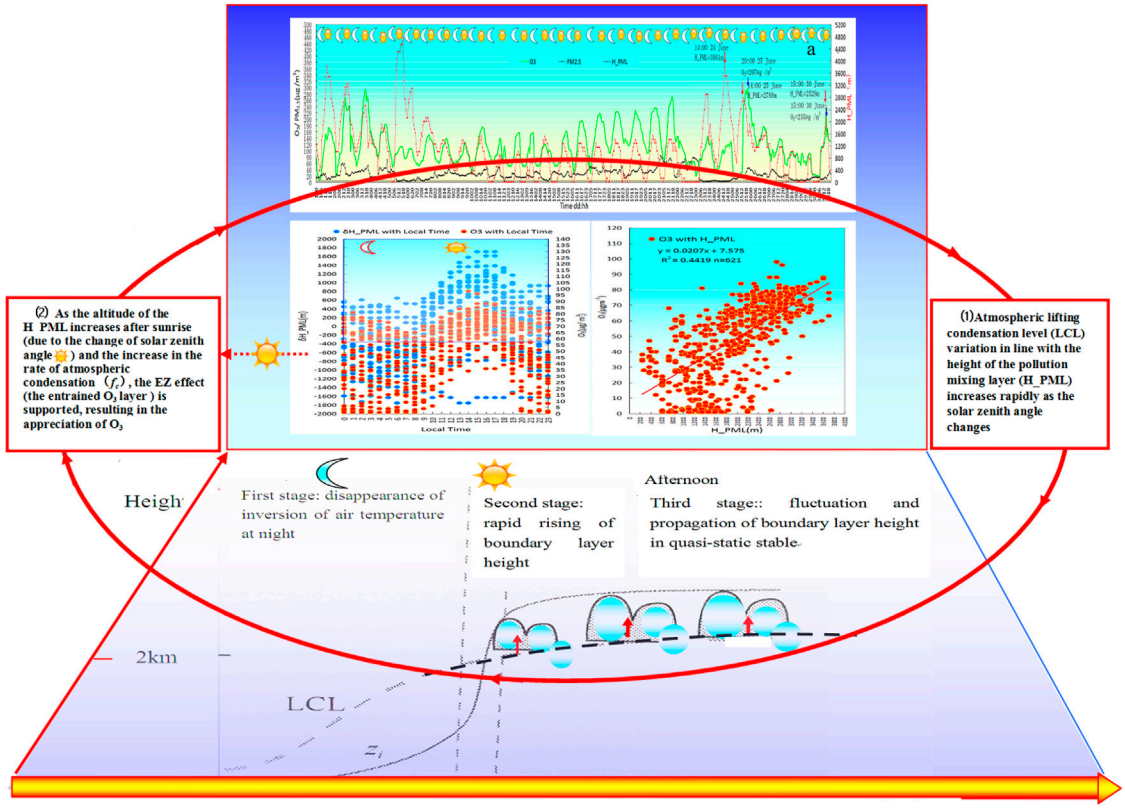

FIGURE 7
Comprehensive physical images of key meteorological factors affecting large increases in the near-surface O_3 concentration entrainment (O_3 EZ) due to variations in solar zenith angle and boundary layer height serve.

As given in Figure 5, an increase in O_3 concentration is caused within a few hours after sunrise. According to an analysis of the meteorological conditions after sunrise, the initial decrease and subsequent increase in NO_2 *versus* O_3 concentration satisfy the law of exponent power rule, according to which seasonal and regional differences in coastal and inland areas depend on coefficients α and β (Wang et al., 2019).

3.3.2 The driving mechanism of meteorological conditions for the EZ effect on the power-exponential growth of O_3 concentration

As can be seen from the discussion in Sections 3.3 and 3.3.1, the power exponential increase in O_3 concentration is due to the decrease of NO_2 as a precursor, that is, the EZ effect that occurs near the boundary layer under the corresponding meteorological conditions. To further reveal the contribution mechanism of the EZ effect and explore the driving factors of meteorological condition, Figure 6A shows the correlation analysis of hourly O_3 and pre-6 h NO_2 concentration in February 2022 in Beijing, and Figure 6B shows the correlation analysis between hourly O_3 and f_c in February 2022 in Beijing. Figure 6 shows the following:

1) Figure 6A shows that February is the winter representative month. As an O_3 precursor, NO_2 showed a significant power exponent negative correlation with O_3 concentration, and the correlation coefficient (R^2) reached 0.33, with a significance level exceeding 0.001, that is, the low value of NO_2 corresponded to the increase in O_3 concentrations after 6 h, which coincides with the period of rise in the height of the mixed layer after sunrise (Figure 6). This implies that the EZ value-added effect is closely related to the exponential increase of O_3 supported by the reduction of NO_2 concentrations.
2) The correlation analysis of the February 2022 hourly resolution O_3 and the f_c observed synchronously (Figure 6B) shows that O_3 increase and f_c positively correlated with the e-exponent, with correlation coefficient (R^2) 0.15, and significance level exceeding 0.01. The threshold (lowest value) of the f_c was 0.7, which coincides with the increase in the O_3 concentration as calculated in Figure 6A, and the decrease in the concentration of the precursor NO_2, whose power exponent value was 0.73. Comparison of Figures 6A,B shows that, the threshold of f_c 0.7 is the

key value of the O_3 precursor NO_2 to the O_3 concentration, that is, to support the value-added EZ effects.

3) As shown in Figure 6C, June is the summer representative month. It is well-known that summer is characterized by a high value of O_3 concentrations everywhere. In June 2022 in Beijing, the O_3 precursor NO_2 was still inextricably bound to the O_3 concentration, the correlation coefficient (R^2) was 0.05, and the level of significance was lower than that in winter. The period of increase in the height of its mixed layer after sunrise also appeared consistently after 6 h. This shows that in summer, even if the O_3 concentration increases considerably, the value-added effect of EZ and the power-exponential growth law of O_3 supported by the reduction of NO_2 concentration still have distinct consistent characteristics.
4) As shown in Figure 6D, the threshold (lowest value) of the f_c in June was 1.85, which is more consistent with the increase in the O_3 concentration calculated in Figure 6C and the decrease in the concentration of the precursor NO_2, and its power exponent value of 0.21 is also more consistent. It shows that the summer threshold of f_c was 1.85 in the hot, high-temperature, and high-humidity summer in Beijing, which is the key value of the O_3 precursor NO_2 to the O_3 concentration and supports the value-added effect of EZ.

Comparative analysis of winter and summer confirmed that the contribution of O_3 precursor NO_2 to the power-exponential increase of the O_3 concentration, as well as the f_c threshold of the adhesion function of the pollution boundary layer, were of great significance in supporting the value-added effect of EZ (Figures 6, 7).

4 Conclusions

The preliminary findings of the current study are as follows.

In this study, the relationships among cloud height and atmospheric condensation rate and solar zenith angle change were discussed by the analysis of information based on the hourly resolution and calculation, and the height change of the mixed layer of atmospheric pollution and its influence on the distribution of the tropospheric O_3 concentration was explored.

1) The results showed that the contribution of O_3 precursor NO_2 to the power-exponential growth of the O_3 concentration is driven by the threshold of f_c growth, due to the lifting of the pollution boundary layer, which has a significant impact on the value-added effect of supporting the EZ.
2) The local day–day cycle change of the height (H_PML) of the atmospheric low-altitude pollution mixing layer and the change during the solar zenith angle contributed significantly to the sharp increase in the surface O_3 concentration. This is the process of photochemical O_3 generation and the cross-effect with the influence of meteorological conditions, resulting in an increase in O_3 concentrations.
3) Another finding of this study provided insight about the development and mechanism of the increase in O_3 concentrations, that is, with the sharp increase in the height of the pollution mixing layer after sunrise, the contribution of the EZ effect (the entrained O_3 layer) to O_3 deposition is actually driven by the high condensation rate (f_c) threshold, which helps the humidification process of O_3 precursors (NO_x), resulting in an enhanced O_3 concentration by the power-exponent law. As shown in the graphical abstract, the process can be summarized as follows: ① atmospheric lifting condensation level (LCL) variation in line with the height of the pollution mixing layer (H_PML) increases rapidly as the solar zenith angle changes. ② As the height of the H_PML increases after sunrise (due to the change of solar zenith angle) and the increase in the rate of atmospheric condensation f_c, the EZ effect is supported, resulting in the appreciation of O_3.
4) The analysis of information during spring, summer, autumn, and winter seasons of the representative stations of Beijing, Hangzhou, Guangzhou, and Sichuan Basin in China further confirmed that with the daytime change of the solar zenith angle, the effect of the micro-physical processes (including the condensation rate threshold drive and the EZ effect) near the pollution mixed-boundary layer (H_PML) on the O_3 concentration increases, thereby indicating its universal significance.

Data availability statement

The original contributions presented in the study are included in the article/Supplementary Material; further inquiries can be directed to the corresponding author.

Author contributions

LL, XZ, and JW designed the research and led the overall scientific questions. YY, WJ, and JZ carried out data processing and analysis. YW and XJ assisted in program and software designing. LL and XZ wrote the first draft of the manuscript, which was revised by JW and XJ. All authors read and approved the final version.

Funding

This research was supported by the Major Project from Natural Science Foundation of China (42090031).

Conflict of interest

The authors declare that the research was conducted in the absence of any commercial or financial relationships that could be construed as a potential conflict of interest.

Publisher's note

References

Albrecht, B., Fang, M., and Ghate, V. (2016). Exploring stratocumulus cloud-top entrainment processes and parameterizations by using Doppler cloud radar observations. *J. Atmos. Sci.* 73, 729–742. doi:10.1175/jas-d-15-0147.1

Andreas, G., and Jochen, S. (2004). Vertical profiles of NO3, N2O5, O3, and Nox in the nocturnal boundary layer2. Model studies on the altitude dependence of composition and chemistry. *J. Geophys. Res.* 109, D12307. doi:10.1029/2003jd004211

Angevine, W. (1997). MErrors in mean vertical velocities measured by boundary layer wind profilers. *J. Atmos.Ocean. Tech.* 14, 565–569.

Bohn, B., Corlett, G. K., Gillmann, M., Sanghavi, S., Stange, G., Tensing, E., et al. (2008). Photolysis frequency measurement techniques: Results of a comparison within the ACCENT project. *Atmos. Chem. Phys.* 8, 5373–5391. doi:10.5194/acp-8-5373-2008

Browning, K. A., Hardman, M. E., Harrold, T. W., and Pardoe, C. W. (1973). The structure of rainbands within a mid-latitude depression. *Q. J. R. Meteorol. Soc.* 99, 215–231. doi:10.1002/qj.49709942002

Gao, S. T., and Zhou, Y. S. (2005). Analyses on warm and humid weather in summer in Beijing and its dynamical identification. *Sci. China* 48, 128–137.

Holmboe, J., Forsythe, G. E., and Gustin, W. (1952). *Dynamic meteorology*. London: Chapman and Hall limited, 363.

Hu, M., Huang, J., Fuentes, J. D., Forkel, R., and Zhang, N. (2016a). Advances in boundary-layer/air pollution meteorology. *Adv. Meteorology* 1, 1–2. doi:10.1155/2016/2825019

Hu, Y. T., Zhao, P., Niu, J. F., Sun, Z. W., Zhu, L. W., and Ni, G. Y. (2016b). Canopy stomatal uptake of NOX, SO2 and O3 by mature urban plantations based on sap flow measurement. *Atmos. Environ.* 125, 165–177. doi:10.1016/j.atmosenv.2015.11.019

Kulmala, M., Vehkamäki, H., Petäjä, T., Dal, M., Lauri, M., and Kerminen, A., (2004). Formation and growth rates of ultrafine atmospheric particles: A review of observations. *J. Aerosol Sci.* 35 (2), 143–176. doi:10.1016/j.jaerosci.2003.10.003

Lenschow, D. H., Paluch, I. R., Bandy, A. R., Thornton, D. C., Blake, D. R., and Simpson, I. (1999). Use of a mixed-layer model to estimate dimethylsulfide flux and application to other trace gas fluxes. *J. Geophys. Res.* 104, 16275–16295. doi:10.1029/1998jd100090

Li, C. H., Meng, J., Guo, L. Y., and Jiang, G. M. (2015a). Effects of ozone pollution on yield and quality of winter wheat under flaxseed competition November 2015. *Environ. Exp. Bot.*, 129–139.

Li, J., Chen, H. B., Li, Z. Q., Wang, P., Cribb, M., and Fan, X. (2015b). Low-level temperature inversions and their effect on aerosol condensation nuclei concentrations under different large-scale synoptic circulations. *Adv. Atmos. Sci.* 32, 898–908. doi:10.1007/s00376-014-4150-z

Madronich, S., and Flocke, S. (1999). "The role of solar radiation in atmospheric chemistry," in *The handbook of environmental chemistry (reactions and processes)*.

Mechergui, R., BenMansoura, A., Laffray, X., Albouchi, A., Akrimi, N., and Garrec, J. P. (2009). Ozone level assessment on the boukornine national park (Tunisia) using plant biomonitoring: Influence of altitudinal parameter and meteorological conditions. *Water Air Soil Pollut.* 204, 285–297. doi:10.1007/s11270-009-0045-5

Shen, X. J., Sj, Y., Zhang, X. Y., Zhang, Y. M., Zhang, L., and Fan, R. X. (2016). Key features of new particle formation events at background sites in China and their influence on cloud condensation nuclei. *Front. Environ. Sci. Eng.* 10 (5), 5–016. doi:10.1007/s11783-016-0833-2

Tang, X. Y., Zhang, Y. H., and Shao, M. B. H. E. P. (2006). *Atmospheric environmental chemistry*, 214–222.

Textor, C., Schulz, M., Guibert, S., Kinne, S., Balkanski, Y., Bauer, S., et al. (2006). Analysis and quantification of the diversities of aerosol life cycles within AeroCom. *Atmos. Chem. Phys.* 6, 1777–1813. doi:10.5194/acp-6-1777-2006

Trousdell, J. F., Conley, S. A., Post, A., and Faloona, I. C. (2016). Observing entrainment mixing, photochemical ozone production, and regional methane emissions by aircraft using a simple mixed-layer framework. *Atmos. Chem. Phys.* 16, 15433–15450. doi:10.5194/acp-16-15433-2016

Wallace, J. M., and Hobbs, P. V. (2006). *Atmosphere science*. 2th ed. New York: Academic Press.

Wang, H. L., and McFarquhar, G. M. (2008). Modeling aerosol effects on shallow cumulus convection under various meteorological conditions observed over the Indian Ocean and implications for development of mass-flux parameterizations for climate models. *J. Geophys. Res.* 113, D20201. doi:10.1029/2008jd009914

Wang, J. Z., Gong, S., Zhang, X. Y., Yang, Y. Q., Hou, Q., Zhou, C. H., et al. (2012). A parameterized method for air-quality diagnosis and its applications. *Adv. Meteorology* 2012, 1–10. doi:10.1155/2012/238589

Wang, J. Z., Yang, Y. Q., Zhang, X. Y., Liu, H., Che, H., Shen, X., et al. (2017). On the influence of atmospheric super-saturation layer on China's heavy haze-fog events. *Atmos. Environ.* 171, 261–271. doi:10.1016/j.atmosenv.2017.10.034

Wang, J. Z., Yang, Y. Q., Zhang, Y. M., Niu, T., Jiang, X. F., Wang, Y. Q., et al. (2019). Influence of meteorological conditions on explosive increase in O3 concentration in troposphere. *Sci. Total Environ.* 652, 1228–1241. doi:10.1016/j.scitotenv.2018.10.228

Wang, S. L., and Chai, F. H. (2002). A study on O3 pollutions in Beijing. *Geo-Science (in Chin.* 22, 360–364.

Webb, A. R., and Steven, M. D. (1986). Daily totals of solar UVB radiation estimated from routine meteorological measurements. *J. Climatol.* 6, 405–411. doi:10.1002/joc.3370060406

Yang, D. S., Liu, Y. B., and Liu, S. K. (1982). *Dynamics of meteorology*. 2th ed., 297–359. Chapter 2.

Zhang, G. Z., Bian, G., Wang, J. Z., and Yang, Y. Q. (2005). The boundary layer chracteristics in the heavy fog formation process over Beijing adjacent areas. *Sci. China* 48, 88–101.

Zhang, X. Y., Wang, Y. Q., Niu, T. Z., Gong, S. L., Zhang, Y. M., and Sun, J. Y. (2005). Atmospheric aerosol compositions in China: spatial/temporal variability, chemical signature, regional haze distribution and comparisons with global aerosols. *Atmos. Chem. Phys.* 12, 779–799.